



Observations of mixed layer restratification by onshore surface transport following wind reversal in a coastal upwelling region

A. C. Dale,^{1,2} J. A. Barth,¹ M. D. Levine,¹ and J. A. Austin³

Received 26 January 2007; revised 5 May 2007; accepted 14 August 2007; published 15 January 2008.

[1] Observations, from the Oregon continental shelf, describe the slumping of a coastal upwelling front in response to a reversal of winds from upwelling- to downwelling-favorable. Initially, the front outcropped in a surface mixed layer of depth 10–20 m with a pronounced cross-shelf density gradient. Following wind reversal, both the unbalanced cross-shelf pressure gradient and wind-driven Ekman transport drove a rapid onshore movement of near-surface water, causing the mixed layer to restratify. At the surface, the cross-shelf density gradient steepened to become a discontinuous front, which propagated onshore at 0.43–0.60 m s⁻¹ as the head of a buoyant gravity current. Internal waves were driven ahead of the front on the base of the former mixed layer. An injected dye tracer revealed that surface water from inshore of the strongest frontal gradient detached from the surface as the gravity current passed over the top of it. This water largely retained the low potential vorticity signature that it had taken on in the mixed layer as it spread across the shelf in a weakly stratified, subsurface layer. Restrartification and frontogenesis were most likely gravity-driven in the first hours following wind reversal, with the contribution from Ekman transport becoming increasingly significant.

Citation: Dale, A. C., J. A. Barth, M. D. Levine, and J. A. Austin (2008), Observations of mixed layer restratification by onshore surface transport following wind reversal in a coastal upwelling region, *J. Geophys. Res.*, *113*, C01010, doi:10.1029/2007JC004128.

1. Introduction

[2] Wind-driven coastal upwelling results from offshore Ekman transport induced by an upwelling-favorable along-shelf wind. Flow divergence at the coast brings the pycnocline to the surface where it outcrops in a zone of cross-shelf density gradient, the “upwelling front,” which separates dense, upwelled water nearshore from lighter water offshore. In regions where upwelling dominates, such as in summer off the west coast of North America, upwelling-favorable winds may be punctuated by periods of weak or reversed winds, during which the coastal ocean “relaxes” from its upwelled state or is forced into downwelling. Events of this type are marked by an onshore movement of surface water, with the lighter offshore water replacing upwelled water nearshore. This cross-shelf transport has significant biological consequences, such as increased coastal barnacle recruitment [*Roughgarden et al.*, 1991]. Knowledge of the physics of relaxation events is limited, however, particularly with respect to the secondary, cross-shelf component of circulation.

[3] An upwelled density structure might be expected to persist during a period of no wind forcing by virtue of the fact that the cross-shelf pressure gradient that it implies is in geostrophic balance with a vertically sheared along-shelf jet. Empirical evidence suggests that, in the interior of the water column, there is a gradual relaxation of such baroclinicity over a relatively long timescale. Off Oregon, this timescale is around 8 d [*Austin and Barth*, 2002]. A quite different regime is expected to exist near the surface at times when strongly upwelling-favorable winds create a mixed layer by direct wind stirring aided by the tendency for offshore Ekman transport to steepen isopycnals. The vertical redistribution of tracers and momentum within the mixed layer prevents a thermal wind balance from being established [e.g., *Tandon and Garrett*, 1995] since wind stress and turbulent momentum transfer are important components of the momentum balance. If the wind stops, the cross-shelf pressure gradient is unbalanced and it drives a sheared flow, tilting isopycnals and restratifying the mixed layer. As the density structure slumps, it seeks a thermal wind balance between the horizontal density gradient and vertically sheared along-front flow induced during the slumping [*Csanady*, 1971; *Tandon and Garrett*, 1995]. Wind forcing and frictional effects can work against the establishment of a balanced final state. Mixed layer instabilities (baroclinic instabilities of the along-shelf flow) may also play a significant role in the restratification [e.g., *Boccaletti et al.*, 2007].

¹College of Oceanic and Atmospheric Sciences, Oregon State University, Corvallis, Oregon, USA.

²Now at Scottish Association for Marine Science, Oban, Argyll, UK.

³Large Lakes Observatory, University of Minnesota, Duluth, Minnesota, USA.

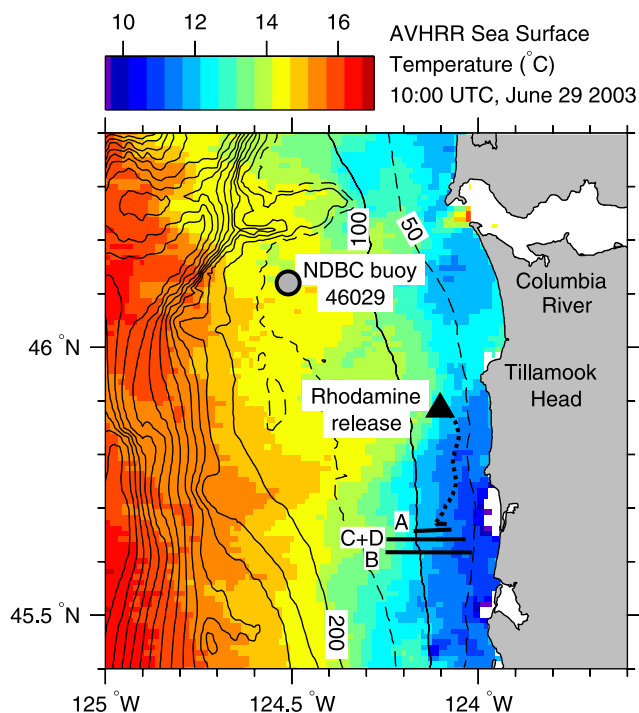


Figure 1. Bathymetry (contoured) of the northern Oregon shelf, showing the location of dye release (triangle), the primary cross-shelf transects (A–D), and NDBC buoy 46029. The contour interval is 100 m (dashed line, 50 m). Underlying is an image of AVHRR sea surface temperature at 1000 UTC on 29 June 2003 (year day 180.42). The dotted line shows the path of a drifter, drogued at 15 m and released with the dye.

[4] Described here are observations from the summer upwelling season of 2003 on the northern Oregon shelf (Figure 1). During a period of strong upwelling-favorable winds (Figure 2) a 10–20 m mixed layer developed, with a cross-shelf density gradient that was especially pronounced at a front marking the edge of less dense offshore water influenced by the Columbia River plume. When winds subsequently reversed, the mixed layer rapidly restratified. An injected dye tracer revealed the evolution of mixed layer water from inshore of the most intense cross-shelf gradient. As the Columbia-influenced water moved onshore, dye-laden water was subducted beneath it. The emphasis in this paper is on describing (section 2) the evolution of the system immediately prior to and following wind reversal, particularly during the 7-h period in which the Columbia-influenced water moved onshore. The dynamics of the restratification are examined (section 3) by comparison with theoretical limiting cases, with the aim of determining the relative importance of gravitational slumping and directly wind-driven transport. The frontogenetic mechanisms by which the plume front intensified, eventually becoming a step discontinuity where surface waters were subducted, are also considered.

[5] In coastal upwelling studies, major simplifications can be made by assuming along-shelf uniformity and effectively reducing the system to two dimensions. The northern Oregon shelf is a region where this assumption seems

reasonable. The coastline is essentially straight, oriented north-south, and this orientation is largely reflected in the bathymetry (Figure 1). In what follows, “cross-shelf” will be assumed equivalent to “east-west” and “along shelf” to “north-south.” There are no major banks or other topographic features. Three-dimensional effects should not be dismissed, however [e.g., *Allen and Kundu, 1978*]. Wind forcing on the Oregon shelf is highly seasonal, being predominantly upwelling-favorable in summer and downwelling-favorable in winter, with a “spring transition” to upwelling-favorable conditions [*Huyer et al., 1979*] of variable timing. As the upwelling season progresses, developing instability of the upwelling front and associated equatorward jet [*Barth, 1994; Durski and Allen, 2005*], lead to meanders, eddies, filaments and other three-dimensional complexity. An additional potential source of three-dimensionality is the freshwater input from the Columbia River, approximately 40 km to the north of the experimental area, and the associated Astoria Canyon. Nevertheless, it is important to the analysis presented here that the situation was, at least locally, two-dimensional during the period described, and this point is discussed further in section 3.2.

2. Observations

[6] Observations were made during the period 26–29 June 2003 from the R/V *New Horizon*. The focus of the experiment was a dye tracer release, one of a series made on the Oregon shelf during the upwelling seasons of 2001–2003. The survey strategy aimed to record the evolution of the dye patch and the system that contained it. In the description that follows, a coordinate system (x, y, z) is adopted, in

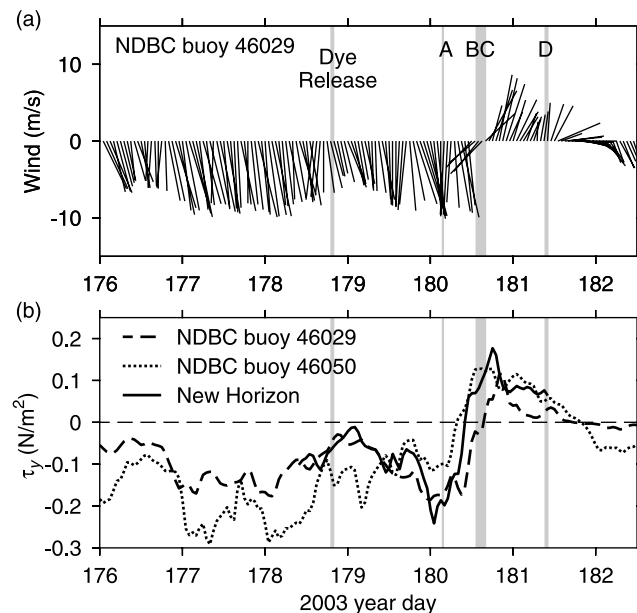


Figure 2. Time series of (a) wind at NDBC buoy 46029 (sticks point downwind) and (b) the northward component of wind stress (τ_y) at buoys 46029, 46050, and the ship. The ship wind record is restricted to the period between the dye release and the end of the observations described in the text. Vertical shaded bars show the time of dye release and of transects A–D.

which axes are directed to the east (onshore), north (along shelf) and upward respectively. Corresponding velocity components are denoted (u , v , w). Times are in 2003 year days, with 26 June being year day 177.

2.1. Dye Release

[7] Experiments involving the subsurface injection of a dye tracer into stratified shelf environments have been described by *Sundermeyer and Ledwell* [2001], *Houghton* [1997], and others. The methods used in the present experiment owe much to those studies. The dye used here was Rhodamine-WT, which is relatively stable when exposed to sunlight [*Smart and Laidlaw*, 1977]. A density-adjusted solution containing 45 kg of dye was injected as a 1.6 km along-shelf streak centered on a depth of 9.7 m and a density of $\sigma_\theta = 25.31$ [*Dale et al.*, 2006]. This was within the pycnocline forming the base of the mixed layer. A drifter, drogued at 15 m, was released with the dye to provide a reference point for dye tracking as well as a quasi-Lagrangian time series tracing the evolution of the system as a whole.

2.2. Survey Techniques

[8] Vertical transects were obtained using a MiniBAT undulating vehicle coupled to a CTD sampling at 8 Hz. The MiniBAT was towed at 6–7 knots (3.1–3.6 m s⁻¹) and undulated between near the surface and 30–50 m with a horizontal separation between dives of 300–900 m (shorter for shallower dives). The vertical sample spacing was 0.3 m or less with the typical spacing being considerably smaller. Transects were mostly oriented east-west (cross-shelf) at various latitudes. For now, it will be implicitly assumed that the features described were uniform in the north-south direction (but see section 3.2). The ship was equipped with a 150-kHz acoustic Doppler current profiler (ADCP) logging in 60-s, 8-m vertical bins with the shallowest centered at a depth of 16 m. Continuous data were also collected from a thermosalinograph, with an intake depth of 2.7 m, and from meteorological sensors.

[9] Detection of the rhodamine dye was by a fluorometer with a freely flushing sensor volume located close to the pumped CTD intake duct. Background fluorescence due to ambient water properties varied by up to 0.025 $\mu\text{g l}^{-1}$ dye equivalent, masking low dye concentrations, however a partial correction for this effect was made by using the strong correlation between background rhodamine fluorescence and transmissometer readings, permitting dye detection to concentrations of around 0.01 $\mu\text{g l}^{-1}$.

[10] To map a rapidly evolving dye patch in a dynamic environment is a considerable challenge. Even in a system that is uniform along-shelf, a patch becomes increasingly dispersed in that direction by shear in the along-shelf velocity. Cross-shelf transects show the distribution of dye particles that have experienced a similar mean along-shelf flow since their release, providing only a partial picture of the dye patch as a whole. Ideally, cross-shelf transects would be made rapidly relative to the timescales on which the system was evolving, and they would span the along-shelf extent of the patch. In the present case, evolution was slow prior to the wind reversal and rapid during the subsequent restratification. The slow prior evolution meant that the dye patch could be thoroughly mapped during that

period, so its state was well known at the time of wind reversal. Following the wind reversal, however, the most interesting period of restratification lasted just 7 h, during which only two cross-shelf MiniBAT transects were obtained. These transects were supplemented at other times by information on frontal gradients at the surface from the ship's thermosalinograph.

2.3. Wind Forcing

[11] Wind time series for the experimental period are available from two National Data Buoy Center (NDBC) buoys, 46029 (60 km to the north of the dye at wind reversal; Figure 1) and 46050 (115 km to the south), and also from the R/V *New Horizon's* own sensors. Qualitatively, changes in wind forcing were similar at all locations (Figure 2). Winds were predominantly along-shelf throughout, being consistently upwelling-favorable (southward) at 5–10 m s⁻¹ for 12 d prior to dye release and for a further 1–1.5 d after dye release before rapidly reversing to downwelling-favorable. The exact timing of the reversal varied with location. The northern buoy lagged the southern buoy by 8 h, nearly half an inertial period, which is a significant duration in the relaxation/restratification process. For this reason, the ship wind record is important, although the ship was moving on a complex path which spanned a 23-km north-south range and between 2.5 and 28 km offshore during the 2-d period centered on the wind reversal. During the period of upwelling-favorable winds, wind stress at the ship was similar to that at the closer, northern buoy (46029), although the timing of the reversal and amplitude of the subsequent stress more closely resembled the southern buoy (46050). In the following analysis, wind stress at the ship will be used, though it should be borne in mind that there was spatial variation in the timing and intensity of the wind events described.

2.4. Summary of Upper-Ocean Evolution

[12] The dye release, at day 178.81, was followed by a brief weakening of upwelling-favorable winds (Figures 2 and 3a), accompanied by onshore motion of the drifter (Figure 3b) and of the surface density structure (not shown). The 16-m ADCP bin also showed a positive onshore velocity (Figure 3c). From day 179.5, the surface density structure moved offshore at a mean velocity of 0.14 m s⁻¹ (determined by a linear regression to the longitude of surface crossings of $\sigma_t = 25$) between day 179.5 and the wind reversal at day 180.42. This offshore motion was presumably the upper expression of an Ekman transport which was also apparent in the 16-m ADCP bin and in the drifter velocity (Figures 3b and 3c). A southward flow component in the 16-m ADCP bin (Figure 3c) weakened from 0.2 m s⁻¹ to 0.1 m s⁻¹ during this period. Deeper flow was to the north (not shown).

[13] The response to wind reversal was rapid. Onshore motion of the surface density structure (described later) was accompanied by onshore flow in the 16-m ADCP bin. The southward flow at 16 m stalled abruptly (see drifter track, Figure 1, and time series, Figure 3), while vertical shear persisted, so flow at 40 m (not shown, but see Figure 8b) was northward at this time. Half a day after wind reversal, the 16-m flow had also become northward. A rapid barotropic response to a change in wind forcing is typical of this

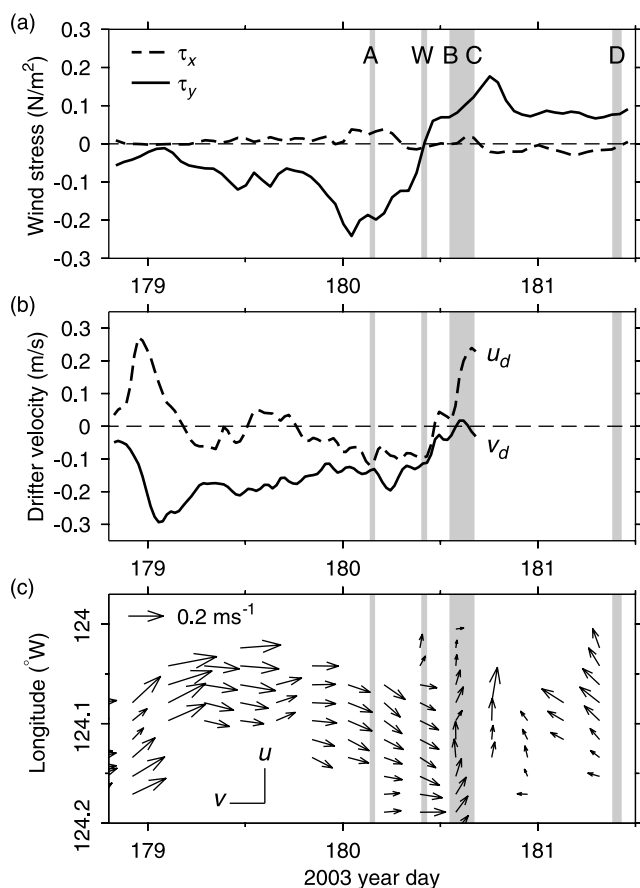


Figure 3. Time series of (a) hourly averaged wind stress components (τ^x , τ^y) (positive east, north) at the ship, (b) drifter velocity (u_d , v_d) (positive east, north), and (c) horizontal current vectors in the 16-m ADCP bin. Vertical shaded bars show the times of transects A–D and of wind reversal (W). The horizontal axis begins at the time of dye injection and drifter release. In Figure 3c, the vertical axis is longitude. Vector orientation is shown by the inset axis (onshore is up). The latitude of observations varies, and observations were gridded such that timescales of less than 0.25 inertial periods and length scales of less than 2 km were neglected.

upwelling system [Smith, 1974]. Throughout the period depicted in Figure 3, the cross-shelf velocity at 40 m was essentially anticorrelated with that at 16 m, with a zero crossing at 20–30 m.

2.5. Prior to Wind Reversal

[14] The initial spreading of the dye patch was described by Dale et al. [2006]. Here, the focus is on the period from the later stages of upwelling-favorable winds, 29 h after release, onward. A survey of the dye patch immediately prior to the wind reversal will be used to describe the dynamical situation at that time (days 180.01–180.32; Figure 4). Winds were strong and to the south, with a mean along-shelf stress $\tau^y = -0.20 \text{ N m}^{-2}$, leading to the development of a mixed layer (transect A in Figure 5) which typically deepened from 10 to 20 m during the survey. Dye was encountered at densities $\sigma_\theta = 24.4$ to 25.6 and longitudes 124.07 to 124.17°W. It had largely been

entrained into the mixed layer (Figure 5). A representative profile (Figure 6) from transect A shows an 18-m, dye-laden mixed layer with dye also detectable in the upper 2 m of the underlying pycnocline, to around 0.1 kg m^{-3} above the mixed layer density (Figure 5).

[15] It will aid later interpretation to establish that the dye patch observed during this period contained all of the dye released and, therefore, provided the source for all dye subsequently observed. By advecting the observations to a common time, the total dye mass present is estimated at $37 \pm 5 \text{ kg}$ with the error bar reflecting uncertainty in gridding the dye field and in removing background fluorescence. Given the other uncertainties of such a calculation this value is not significantly different from the 45 kg of dye released.

[16] Since the temperature, salinity and dye concentration of the mixed layer were near-uniform vertically, it is tempting to assume that the velocity structure was similarly uniform (slab-like) at this time. This may not be the case, however, for reasons summarized by Young [1994]. Observations from several upwelling regions [Lentz, 1992] have shown slab-like cross-shelf velocity structure in the mixed layer, but vertical shear in the along-shelf velocity, taking the form of a wind-driven surface log layer. The only information available concerning the mixed layer velocity prior to the wind reversal is the observation that the surface density structure moved offshore at 0.14 m s^{-1} (section 2.4). A 10-m slab at this velocity yields an offshore transport of $1.4 \text{ m}^2 \text{ s}^{-1}$ which accounts for most of the theoretical (steady) Ekman transport ($\tau^y/\rho_0 f = 1.88 \text{ m}^2 \text{ s}^{-1}$). Since the

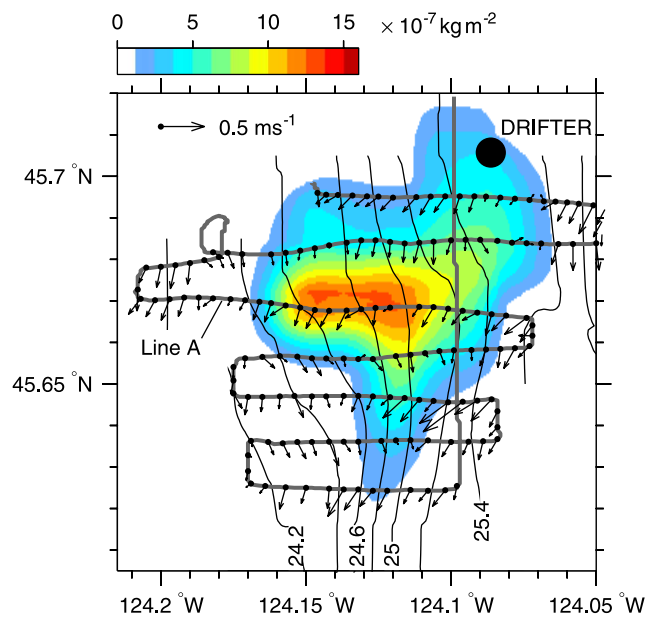


Figure 4. Dye load of the water column (shaded) in the period immediately preceding wind reversal (days 180.01–180.32). The survey path is dark gray. Contours show near-surface density from the R/V *New Horizon* flow-through system. Vectors are 2-min averaged ADCP velocities in an 8-m vertical bin centered at 16 m. All observations have been advected to a common time (day 180.17) by assuming a spatially and temporally constant velocity during this period.

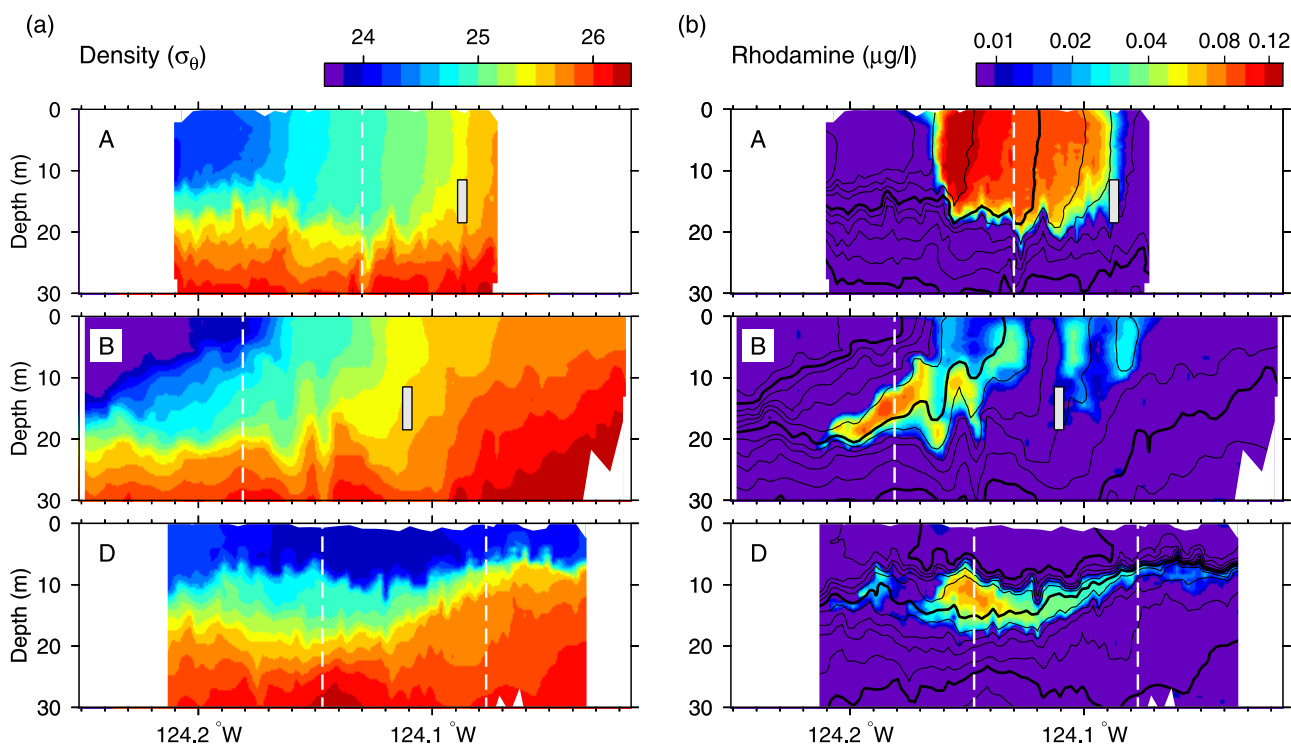


Figure 5. Cross-shelf sections of (a) density (σ_θ) and (b) rhodamine concentration ($\mu\text{g/L}$) (log scale) on transects A, B, and D, surveyed 6.0–5.1 h before, 3.1–4.7 h after, and 23.1–24.7 h after wind reversal, respectively. Vertical white boxes show the longitude and depth span of the drifter drogue at the time of each transect (latitude was different). Dashed lines show the profiles of Figure 6.

depth of the mixed layer increased during this period, its density would also have been influenced by entrainment. The drifter, with a 7-m drogue centered at 15 m, moved offshore at a mean velocity of 0.08 m s^{-1} and the 8-m ADCP bin centered at 16 m had a mean offshore component of 0.04 m s^{-1} . Both of these measures presumably represent a combination of the mixed layer velocity and the shear layer beneath it.

[17] Immediately following the survey of Figure 4, a single CTD cast was made at 124.30°W (day 180.37), 6.8 km west of the offshore end of transect A. During transit to and from this station, the ship flow-through system revealed an intensification of the cross-shelf density gradient centered on $\sigma_\theta = 24$ and latitude 124.24°W (Figure 7). This gradient marked the edge of the relatively warm, fresh offshore water influenced by the Columbia plume and was offshore of the dye patch. The CTD cast showed a 15 m mixed layer in this Columbia-influenced water. Whether the zone of maximum cross-shelf surface density gradient was also mixed to a similar depth is not known.

2.6. Wind Reversal and Restratification of the System

[18] Reversal of the along-shelf component of wind stress at the ship occurred at day 180.42. The inertial period T (16.8 h at this latitude) provides a timescale for the subsequent restratification. Cross-shelf MiniBAT transects show the density structure (Figure 5a) and dye concentration (Figure 5b) shortly (relative to an inertial period) after wind reversal (transect B) and more than an inertial period after wind reversal (transect D). Additional transects C and E immediately followed B and D respectively.

[19] Transect B was run in an offshore direction from 3.1 to 4.7 h (0.19 to 0.28 inertial periods) following wind reversal. The mixed layer of transect A had begun to restratify via a vertically sheared (surface-intensified) onshore flow. This is also hinted at in the ADCP velocity (Figure 8), although the shallowest data available are from the 8-m bin centered at 16 m. The front bounding the Columbia-influenced water had slumped, with its surface expression moving rapidly onshore and steepening from a smooth intensification of the cross-shelf density gradient to a discontinuous step of around 0.9 kg m^{-3} on transect B (Figure 7). The base of the front (its intersection with the base of the former mixed layer) did not move greatly cross-shelf between transects B and C (Figure 8). The dye patch on transect B extended to the surface inshore of the surface front, but was entirely subsurface offshore of it (Figures 5 and 6). The wedge of light water was apparently riding over the top of the dye patch which separated from the surface at the front.

[20] Following transect B, a short leg of 1.5 nm (2.8 km) was made to the north, before turning onshore on transect C. The time lag between B and C (time interval at a given longitude) ranged from 0.3 to 2.8 h. The surface front was encountered farther onshore on transect C than on transect B (Figure 7), with the displacement between these two crossings implying an onshore propagation at 0.60 m s^{-1} assuming along-shelf uniformity. On transect C, the slumping wedge of Columbia-influenced water (shaded in Figure 8) was beginning to resemble a classic gravity current with its head, at the surface front, leading a plume of relatively uniform thickness (around 6 m). The onshore

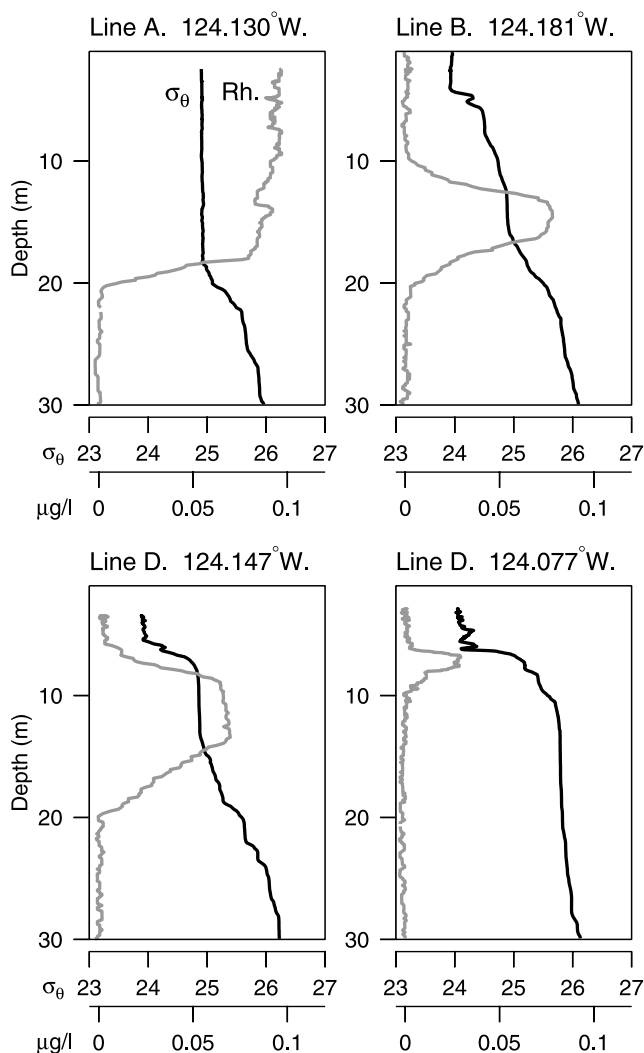


Figure 6. Profiles of density (σ_θ , black lines) and rhodamine concentration ($\mu\text{g/L}$, shaded lines) at locations shown in Figure 5.

velocity in the 16-m ADCP bin beneath the surface front and above the deeper pycnocline had intensified to 0.22 m s^{-1} (the mean within a 5 km bracket spanning the frontal location). The north-south velocity of this water was small, in contrast to the stronger northward flow beneath the pycnocline.

[21] On both transects B and C, undulations of the pycnocline at 20 m were seen inshore of the surface front (Figure 8). These features appear to have been internal waves traveling onshore ahead of the front. Peak-to-trough amplitudes were up to 8 m. Although the up-down cycles of the MiniBAT did not fully resolve these waves, the consistency of their apparent shape between the two east-west transects suggests that they were resolved at least marginally. To explore these oscillations more closely, the depths of crossings of the $\sigma_\theta = 25.5$ isopycnal were extracted from the raw MiniBAT record, and a cubic spline fitted to these points (Figure 9). Estimates of the propagation speed c of the disturbance are possible by two different methods. First, the onshore displacement between the observations on

transects B and C gives $c = 0.55 \text{ m s}^{-1}$. Second, the dilation in spacing of the two wave troughs due to the fact that the observations were made from a moving ship (effectively a Doppler shift) also permits an estimate of speed. The predicted dilation factor is

$$\alpha = \frac{s_C(s_B + c)}{s_B(s_C - c)}, \quad (1)$$

where s_B and s_C are the ship speed on transects B and C respectively, and c is the speed at which the disturbance was traveling onshore. On the basis of the spline fit, $\alpha = 1.31$, which yields $c = 0.45 \text{ m s}^{-1}$. The relative consistency of the two estimates of c bolsters confidence that the shape of the disturbance was well represented.

[22] Transect D was also run in an offshore direction, from 23.1 to 24.3 h (1.38 to 1.45 inertial periods) following wind reversal. At this time, the dye patch was entirely subsurface, capped by the lighter Columbia-influenced water (Figure 5). The surface density was relatively uniform across the shelf and no longer increased monotonically onshore. The inshore edge of the Columbia-influenced water was not observed. An extrapolation of the frontal locations of Figure 7 suggests that the front had reached the coast around 13 h after wind reversal. The strongest dye concentrations occurred in a weakly stratified core of around 5 m thickness, centered close to 124.15°W (Figure 6). Dye also penetrated the more stratified waters above and below, weakening away from the core, but significantly nonzero over a 13-m vertical range (7–20 m depth). The dye layer extended onshore, gradually thinning, weakening and becoming denser (Figure 5). At its inshore end, it had a thickness of 1–2 m and lay immediately beneath an intense pycnocline, but still appeared to retain its weakly stratified signature (Figure 6). Analysis in section 3.6 will compare the change in the stratification of the dye patch with that expected during a potential vorticity conserving geostrophic adjustment.

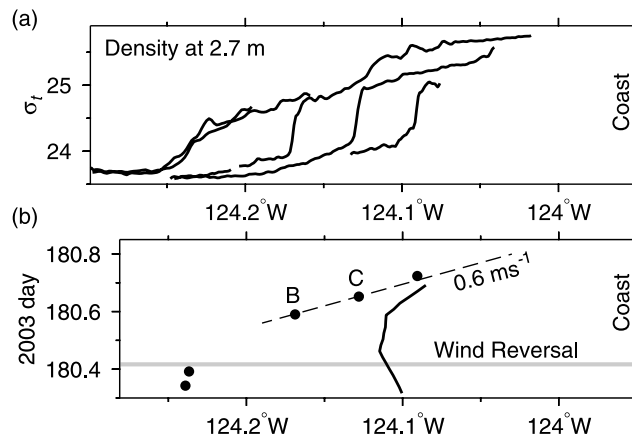


Figure 7. (a) Frontal propagation across the shelf, as seen in near-surface density on five east-west transects, from the R/V *New Horizon* thermosalinograph. The coast is at 123.95°W . Frontal propagation is from west to east. (b) Times of the frontal crossings. See Figure 11 for locations. The solid line indicates the drifter longitude.

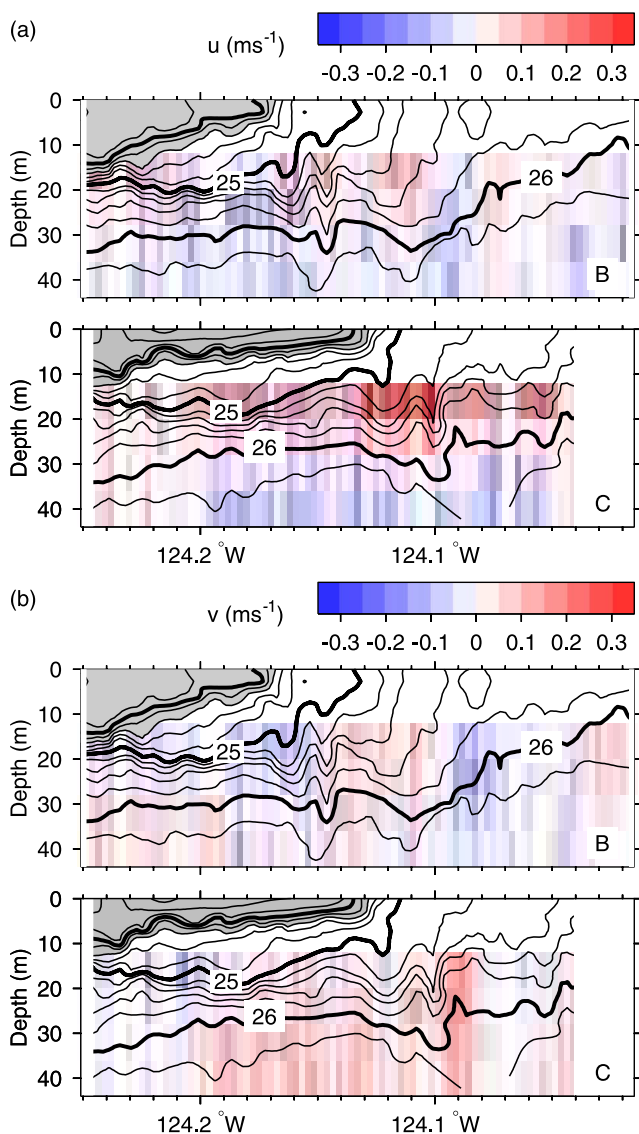


Figure 8. (a) Eastward (u) and (b) northward (v) ADCP velocity components on transects B and C. Density (σ_θ) is contoured, with shaded areas representing $\sigma_\theta < 24.4$, the wedge of Columbia-influenced water.

2.7. Density Evolution of the Dye Patch

[23] The density distribution of the dye patch $\phi(\sigma_\theta)$ has been estimated in three time intervals containing transects A, B + C and D + E (Figure 10) (ϕ_A is calculated from the entire survey of Figure 4 whereas ϕ_{BC} and ϕ_{DE} are both calculated from just these pairs of east-west transects). Additionally, an estimate of the initial density distribution $\phi_0(\sigma_\theta)$ is based on the density measured during dye injection. Early encounters with the dye patch suggest that ϕ_0 is a good representation of the initial dye distribution, with a mean of $\sigma_\theta = 25.27$. ϕ_A , ϕ_{BC} and ϕ_{DE} are considerably broader distributions, with means $\sigma_\theta = 25.07$, 25.15 and 25.08 respectively. Entrainment into the mixed layer occurred between ϕ_0 and ϕ_A , so the decrease in mean density of the patch is consistent with it mixing with less dense overlying water. The restratification occurred between ϕ_A and ϕ_{DE} . Changes in the density distribution

during this period cannot be distinguished from uncertainties due to survey bias. There was clearly much less mixing of the dye-laden water during the restratification process than during the initial entrainment into the mixed layer.

3. Dynamics of the Restratification

3.1. Mechanisms

[24] In response to the weakening and reversal of the upwelling-favorable wind, a surface-intensified onshore flow led to a restratification of the mixed layer. Two mechanisms that would drive such a flow are a directly wind-driven response to downwelling-favorable winds, and a gravity-driven slumping due to imbalance in the cross-shelf pressure gradient when wind stirring weakened. An important distinction between these mechanisms is that the former requires a wind reversal whereas the latter requires a weakening of the wind.

[25] The observations are now compared with the theoretical behavior of a number of simplified systems. Following an investigation of the two-dimensional assumption (section 3.2), a purely wind-driven transport is considered (section 3.3) and compared with the actual onshore transport of Columbia-influenced water (section 3.4). The observed slumping of isopycnals is then compared with a frictionless geostrophic adjustment driven by an unbalanced pressure gradient (section 3.5). An unforced, frictionless slumping would conserve potential vorticity, whereas a wind-driven process would not. Although potential vorticity cannot be calculated directly, the change in stratification of the dye patch is compared with that expected during a potential vorticity conserving geostrophic adjustment (section 3.6). Finally, comparisons are made with gravity current theory (section 3.7), which is appropriate when there is a discontinuity in density between the buoyant onshore flow and the ambient water over which it flows. The rate of advance of a gravity current is controlled by processes at its head (the front). Also considered (in section 3.5) are the frontogenetic

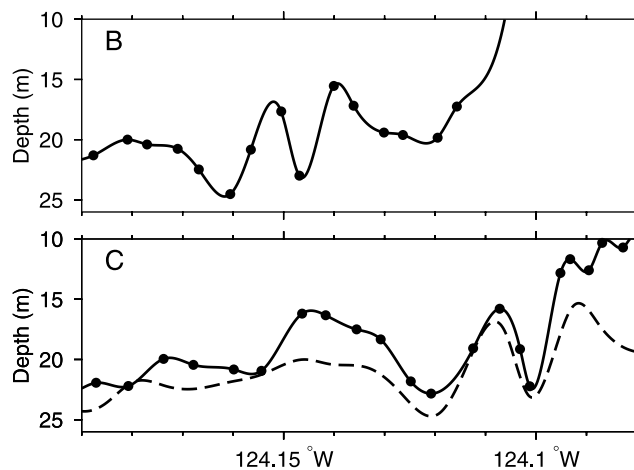


Figure 9. Depth of the $\sigma_\theta = 25.5$ isopycnal on transects B and C. Bullets show actual MiniBAT crossings of this density surface. Curves are a cubic spline fit to these points. The dashed line shows the spline fit for transect B translated and dilated by a factor $\alpha = 1.31$ so that the two major wave troughs coincide.

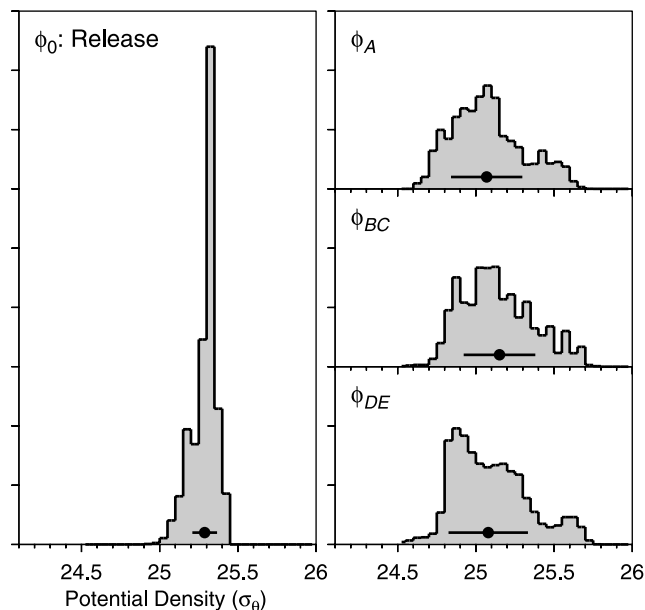


Figure 10. Histograms of the distribution of observed dye in density space at release (ϕ_0), prior to wind reversal (ϕ_A), during restratification (ϕ_{BC}), and postrestratification (ϕ_{DE}). Distributions are normalized such that they have equal area, so vertical axes are dimensionless. Bullets and bars above the density axis show the mean and standard deviation of each distribution.

mechanisms which intensified gradients at the head of the Columbia-influenced water in the early stages of its onshore advance.

3.2. Assumption of Two-Dimensionality

[26] It has been implicitly assumed that along-shelf gradients were weak during the experimental period, and that the dynamics of the evolution of the system can be adequately described in just the two dimensions of a vertical slice normal to the coastline and topography. Although this assumption is clearly an approximation, there is considerable evidence to suggest that, in this case, it is a reasonable approximation. Certainly, the rather straight coastline and shelf bathymetry are conducive to along-shelf uniformity of ocean properties. The assumption that the slumping front was oriented along-shelf, and advanced directly onshore, is now examined.

[27] The only high-quality sea surface temperature image from the period was obtained at day 180.42 (Figure 1), coincident with the wind reversal. At this time, no major mesoscale eddies or filaments were apparent, and temperature essentially increased monotonically offshore. The temperature gradient $|\nabla T|$ estimated from this image (Figure 11) reveals that frontal features were patchy. A pool of relatively cool water was against the coastline to the south of Tillamook Head (45.95°N). Such features are commonly observed south of capes during the upwelling season [Kelly, 1985] due to the separation of equatorward flow from the coast. The offshore boundary of this “cool pool” was the front of interest here. Propagating surface gravity current fronts have a tendency to form cusps in regions where their initial horizontal shape is concave

[Cooper et al., 2001]. Such complexity would clearly confound an estimate of propagation speed based on two-dimensional assumptions. Fortunately, the initial shape of the front (assumed to be the 13°C isotherm in Figure 11) was locally slightly convex in the region of interest with an essentially north-south orientation on the larger scale. The possibility of developing three-dimensionality due to baroclinic instability of the front should not be dismissed, although this occurs on inertial and longer timescales [Boccaletti et al., 2007].

[28] The fact that the ship’s encounters with the front show a relatively consistent onshore advance from the time of wind reversal (Figure 7), despite the fact that these encounters occurred at varying latitudes, supports a north-south orientation of the front. A more careful analysis can be made of the three frontal crossings during the period of rapid onshore propagation. If it is assumed that the surface front was linear and oriented at an angle θ from north (positive clockwise), its propagation speed c can be determined from any pair of fixes as a function of the unknown θ . For two observations separated by a horizontal displacement (Δx , Δy) and a time Δt ,

$$c(\theta) = \frac{\Delta x \cos \theta - \Delta y \sin \theta}{\Delta t}. \quad (2)$$

Three fixes on the front allow two independent estimates of $c(\theta)$, and the intersection (c , θ) gives values that are consistent with all three fixes. This procedure yields $c = 0.43 \text{ m s}^{-1}$ and $\theta = 14^\circ$. The three frontal crossings could equally be explained by a front that was oriented exactly

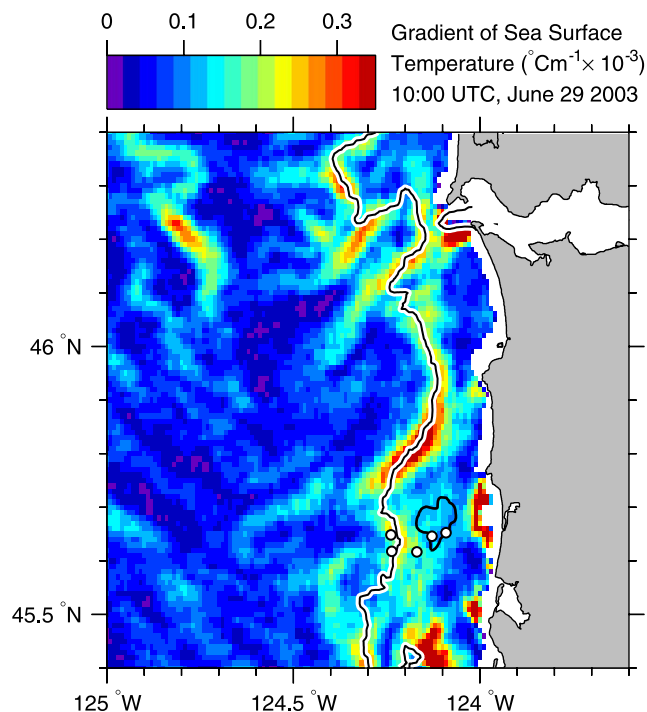


Figure 11. Sea surface temperature gradient $|\nabla T|$ at day 180.42, based on the image of Figure 1. The $T = 13^\circ\text{C}$ contour is shown, as is the extent of the dye patch depicted in Figure 4 (bold line). Open circles show the locations of the frontal crossings depicted in Figure 7.

north-south, but decelerated from $c = 0.60 \text{ m s}^{-1}$ between the first two crossings to $c = 0.48 \text{ m s}^{-1}$ between the second two. The range of these values, $c = 0.43\text{--}0.60 \text{ m s}^{-1}$, is taken as an estimate of the uncertainty in the propagation speed of the front due to orientation and temporal variability. Subject to this uncertainty, the two-dimensional approximation seems locally reasonable.

3.3. Wind-Driven Transport Estimates

[29] A naive calculation of a steady onshore Ekman transport during the period of transects B and C is $U = \tau^y / f\rho_0 = 1.03 \text{ m}^2 \text{ s}^{-1}$ ($\tau^y = 0.11 \text{ N m}^{-2}$). This only provides around one third of the transport inferred from the advance of light surface water across the shelf (a 6-m slab of water advancing at $c = 0.43\text{--}0.60 \text{ m s}^{-1}$, gives $U = 2.58\text{--}3.60 \text{ m}^2 \text{ s}^{-1}$). However, since the observed transport occurred within the first inertial period of wind reversal, a more careful, time-dependent calculation is warranted in order to include adjustment processes.

[30] The wind-driven component of transport is modeled by assuming horizontal uniformity, following *Pollard and Millard [1970]*. Momentum equations are

$$\frac{\partial u}{\partial t} - fv = \frac{1}{\rho_0} \frac{\partial \tilde{\tau}^x}{\partial z} \quad (3)$$

$$\frac{\partial v}{\partial t} + fu = \frac{1}{\rho_0} \frac{\partial \tilde{\tau}^y}{\partial z}, \quad (4)$$

where stress terms ($\tilde{\tau}^x, \tilde{\tau}^y$) represent Reynolds stresses in the (x, y)-directions. Integrating vertically from the surface to a level beneath significant wind-induced stress ($z = -H$), and defining $(U, V) = \int_{-H}^0 (u, v) dz$ to be the wind-driven transport,

$$\frac{\partial U}{\partial t} - fV = \frac{\tau^x}{\rho_0} - aU \quad (5)$$

$$\frac{\partial V}{\partial t} + fU = \frac{\tau^y}{\rho_0} - aV, \quad (6)$$

where (τ^x, τ^y) is the wind stress at the surface ($z = 0$). Ad hoc terms have been added to damp (U, V) over a timescale $1/a$, set here to 4 d [*D'Asaro, 1985*]. In a steady state ($\partial/\partial t = 0$) with $a = 0$, equations (5) and (6) reduce to the Ekman transport

$$(U, V) = \frac{(\tau^y, -\tau^x)}{f\rho_0}. \quad (7)$$

A time-dependent solution $U(t)$ is obtained by numerically integrating equations (5) and (6) from an initial time $t = t_0$ subject to the observed wind stress. The cumulative cross-shelf transport $\hat{U}(t)$ is defined as

$$\hat{U}(t) = \int_{t_0}^t U(t') dt'. \quad (8)$$

[31] In order to represent the offshore transport that existed before the wind reversal, t_0 is taken to be day 180.20, 5 h prior to wind reversal. The mean wind stress $(\tau^x, \tau^y)(t_0) = (0.030, -0.172) \text{ N m}^{-2}$ over the 5-h period prior to t_0 determines an initial $(U, V)(t_0)$ (from equation (7)). Note that $\hat{U}(t)$ is not set to zero at $t = t_0$ but at a later reference time (described in section 3.4).

[32] The cross-shelf transport $U(t)$ reverses at the minimum of $\hat{U}(t)$ in Figure 12. This reversal lags wind reversal as the initial offshore transport adjusts. Inertial oscillations are set up. In the undamped case, reversal of $U(t)$ lags the wind by 2.4 h (0.14 inertial periods). In the damped case, the lag is 0.9 h (0.05 inertial periods). The inertial oscillations periodically enhance onshore transport, so at times U exceeds the steady Ekman transport equation (7). For comparison, the cross-shelf velocity of the drifter (drogued at 15 m) reversed between 1 and 1.5 h after wind reversal at the ship (Figures 12 and 3).

3.4. Transport Estimates From Density Sections

[33] For comparison with the predicted wind-driven transport, a cumulative cross-shelf transport can be estimated from the MiniBAT density transects. In order to fully represent the onshore transport following the wind reversal, a reference time and longitude are set to correspond to a frontal crossing close to the time of wind reversal, specifically, a crossing of the $\sigma_\theta = 24.4$ isopycnal at day 180.39, 0.6 h before wind reversal (the second frontal crossing of Figure 7). A proxy for the cumulative onshore transport is then the quantity of water lighter than $\sigma_\theta = 24.4$ that was subsequently observed inshore of this longitude. This water corresponds to the Columbia-influenced surface water and presumably represents most of the wind-driven transport through the reference longitude. The inshore edge of the $\sigma_\theta < 24.4$ water was only observed on transects B and C, so estimates of cumulative transport are only possible in these two cases. A third, cautious estimate is made by extrapolating a linear regression fit between cumulative transport and frontal position for transects B and C to an additional frontal crossing (the final crossing of Figure 7). The two cumulative transport estimates appear in Figure 12 as black circles, whereas the extrapolated value is shaded.

[34] In order to make direct comparisons with the wind-driven transport estimates, a constant offset is applied to $\hat{U}(t)$ such that $\hat{U}(t) = 0$ at day 180.39, the reference time for the density-based estimates (Figure 12). With this correction, it is noted that the density-based transport estimates exceed the wind-driven estimates $\hat{U}(t)$ (density-based estimates in Figure 12 lie above the curves of $\hat{U}(t)$). At the time of the frontal crossing on transect C, the cumulative onshore transport inferred from the hydrographic section is 4.09 m^2 . The (damped) wind-driven estimate is 1.71 m^2 . Without damping, the later reversal of the cross-shelf transport means that the cumulative wind-driven transport estimate at the time of C is just 0.57 m^2 , although the instantaneous mass flux at that time (gradient of $\hat{U}(t)$ in Figure 12) is similar to that inferred from the density sections. This high wind-driven flux is attained because the onshore transport is enhanced by inertial oscillations set up by adjustment of the offshore transport that existed prior to the wind reversal. The enhancement is greatest in the undamped calculation, but the lack of damping means that the transport reversal in this

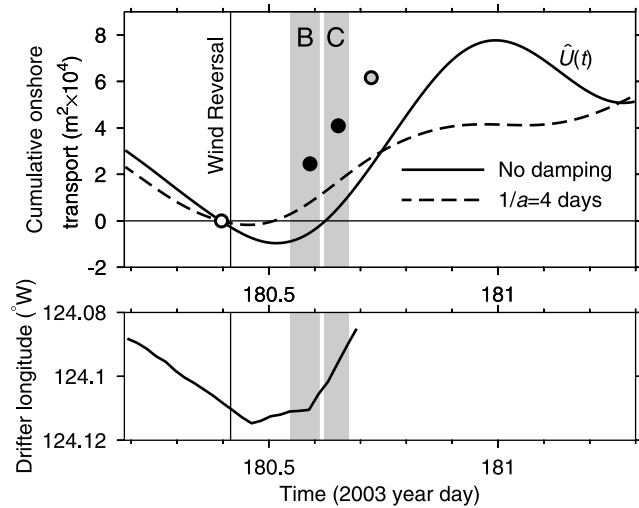


Figure 12. Cumulative wind-driven cross-shelf transport $\hat{U}(t)$ resulting from the north-south component of R/V *New Horizon* wind stress. Calculations are undamped (solid line) and damped with a timescale of 4 d (dashed line). Black circles show the estimated transport from hydrographic sections. The shaded circle is inferred from an additional frontal crossing (see text). All transports are offset to zero at the reference time, day 180.39 (open circle). Shaded bars show the times of transects B and C. The lower panel shows the drifter longitude.

case comes too late to account for the cumulative transport seen in the density sections. There appears to be no way that wind forcing can account for the onshore transport that occurred soon after wind reversal.

3.5. Geostrophic Adjustment and Frontogenesis

[35] In the frictionless, unforced geostrophic adjustment of a front, cross-frontal motion is driven by an unbalanced pressure gradient in that direction and evolution of the density and velocity structure conserves potential vorticity. Consider (following *Tandon and Garrett* [1994]) a slab of fluid of depth H on an f -plane, bounded above and below by rigid, horizontal surfaces. The fluid is initially ($t = 0$) at rest and has a vertically uniform density that increases linearly in x ($M^2 = g/\rho_0 \partial\rho_i/\partial x$ is constant, where $\rho_i(x)$ is the initial density distribution). The pressure gradient $\partial p/\partial x$ is zero at the mid-depth, for reasons that will be discussed later. Isopycnals pivot about the mid-depth, with the time-dependent horizontal displacement s of a particle on the upper boundary being

$$s = \frac{HM^2}{2f^2}(1 - \cos ft) \quad (9)$$

(for derivation, see *Tandon and Garrett* [1994]). Particles on the bottom boundary have a displacement that is equal and opposite to particles at the surface. As isopycnals slump, a vertically sheared along-shelf velocity v develops. The change in v over some time interval is related to cross-shelf particle displacement by

$$\Delta v = -f\Delta x \quad (10)$$

(an integral of the along-shelf momentum equation). Because the problem has no x -dependence, the horizontal density gradient remains constant in z and t . There is no velocity divergence and consequently no vertical velocity.

[36] The endpoint of a geostrophic adjustment is a state in steady geostrophic equilibrium satisfying the thermal wind balance:

$$\frac{\partial v}{\partial z} = -M^2/f; \quad u = 0. \quad (11)$$

However, this state has less energy than the system had initially. In the *Tandon and Garrett* [1994] solution, the vertical shear $\partial v/\partial z$ matches the thermal wind state (equation (11)) after a quarter of an inertial period ($t = \pi/2f \equiv T/4$), but u is nonzero at this time so the density structure continues to slump. The system oscillates about this state with the inertial period. Endpoints of the oscillation are the initial (unstratified) state and one in which $\partial v/\partial z$ and $\partial\rho/\partial z$ are twice those of the thermal wind balance. Energy loss, for instance by radiation of internal waves, permits less idealized systems to converge on the thermal wind state.

[37] *Tandon and Garrett* [1995] considered cases in which a mixed layer with a horizontal density gradient was created by mixing to some depth the density and velocity structure of a baroclinic front that was previously in geostrophic balance (their cases II and III). In these scenarios, there is always a level within the mixed layer that remains in geostrophic balance when the water column is mixed. Isopycnals pivot about this level during restratification. When $\partial\rho/\partial x$ is uniform in z , this level is the mid-depth of the mixed layer. There may be no net cross-frontal transport during restratification, as the cross-frontal flow above and below the balanced level has opposite sign. An additional complexity is that the lower boundary of the mixed layer is not rigid, and may deform during restratification.

[38] An estimate of the maximum cross-shelf density gradient observed prior to wind reversal (Figure 13) is $\partial\rho_i/\partial x = 3.2 \times 10^{-4} \text{ kg m}^{-4}$. In the *Tandon and Garrett* [1994] solution, this gradient would imply (from equation (9) with $H = 15 \text{ m}$) a displacement of the top of the initial mixed layer relative to the bottom ($2s$) of 4.2 km at the time of the frontal crossing on transect B, assuming that slumping started at the time of wind reversal. The relative displacement observed on transect B was 5.5 km. This frontal crossing occurred 4.2 h after wind reversal, approximately a quarter of an inertial period. Since the dye patch lay inshore of the strongest cross-shelf density gradient and had a typical $\partial\rho_i/\partial x = 1.4 \times 10^{-4} \text{ kg m}^{-4}$, a dye-laden water column would (again, from equation (9)) have slumped to a relative displacement ($2s$) of 1.9 km at the time of transect B.

[39] The fact that the observed density gradient was not uniform in x is significant. Since the particle displacements (equation (9)) and the rate of slumping in the *Tandon and Garrett* [1994] solution scale as $\partial\rho_i/\partial x$, a nonzero $\partial^2\rho_i/\partial x^2$ implies water columns slumping at different rates, leading to horizontal divergence and vertical stretching (Figure 14). Applying equation (9) beyond its strict requirement of no horizontal divergence predicts the intensification of surface density gradients on the dense side of the strongest initial

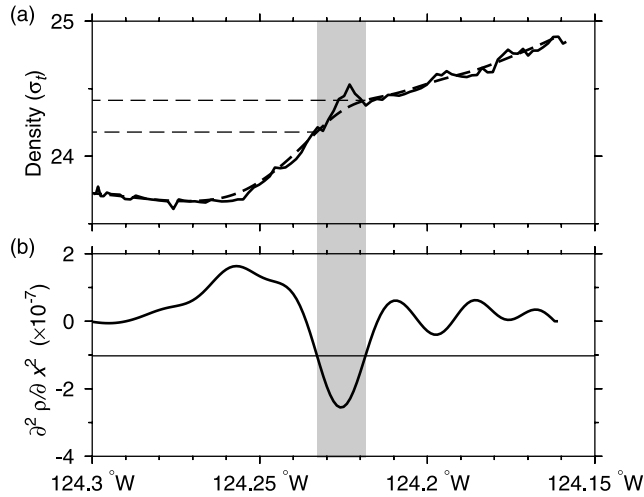


Figure 13. (a) Near-surface density of the front observed during transect A (dashed line is smoothed). The frontal crossing was at day 180.39, prior to wind reversal. (b) $\partial^2 \rho_i / \partial x^2$ of the smoothed density. The horizontal line shows $-2f^2 \rho_0 / gH$, and the region where $\partial^2 \rho_i / \partial x^2 < -2f^2 \rho_0 / gH$ is shaded.

density gradient to the point of discontinuity when $\partial s / \partial x < -1$, or (at $t = T/4$):

$$\frac{\partial^2 \rho_i}{\partial x^2} < -\frac{2f^2 \rho_0}{gH}. \quad (12)$$

This condition actually has more general significance, as the condition under which discontinuities necessarily arise in the geostrophic adjustment of any initial $\rho_i(x)$ [Ou, 1984].

[40] Estimates of $\partial^2 \rho_i / \partial x^2$ prior to wind reversal (Figure 13) show a 1.2 km region on the inner flank of the front, centered on a density $\sigma_t = 24.33$, where equation (12) holds. The $\partial^2 \rho_i / \partial x^2$ minimum at the surface marks the water parcel where discontinuity would first arise. By $t = T/4$ (4.2 h), equation (12) implies that water within the entire shaded band of Figure 13 would have been overrun by lighter water, so this density range would be absent from the surface. The density step seen 4.2 h after wind reversal (Figure 7) was centered close to $\sigma_t = 24.33$, as expected, although it spans a density range (0.9 kg m^{-3}) that is substantially larger than the shaded density range of Figure 13 (0.24 kg m^{-3}). It was noted earlier that the density on each side of the step increased with time. On the dense side of the front, this is consistent with the lighter water overrunning increasingly dense water. On the less dense side of the front, it may represent entrainment of denser fluid across the step.

[41] In conclusion, the simple *Tandon and Garrett* [1994] model predicts rather well (slightly underestimates) the initial slumping of the most intense cross-shelf density gradient. Also predicted is the steepening of frontal gradients, eventually leading to a discontinuity of surface density and subduction of water from the inshore flank of the front. This is a result with significance beyond the scope of the Tandon and Garrett solution, which strictly does not apply when frontal gradients are not uniform [Ou, 1984].

3.6. Potential Vorticity Considerations

[42] An unforced, frictionless geostrophic adjustment conserves potential vorticity. The extent to which stratification increases as the density structure slumps is effectively limited by the initial potential vorticity which defines the ultimate thermal wind balance. The change in stratification of the evolving dye patch is now examined and compared with a potential vorticity conserving restratification process.

[43] Assuming along-shelf uniformity ($\partial / \partial y = 0$), potential vorticity (Q) can be expressed in the form

$$Q = (f + \partial v / \partial x) N^2 + \partial v / \partial z M^2, \quad (13)$$

where N is the buoyancy frequency ($N^2 = -g / \rho_0 \partial \rho / \partial z$) and M is its horizontal analog ($M^2 = g / \rho_0 \partial \rho / \partial x$). Q is conserved, unless the curl of the frictional stresses has a component that is not directed along-shelf [e.g., *Pedlosky*, 1979]. So, for instance, Q is modified by an along-shelf wind stress, or by internal stresses related to vertical shear in the along-shelf velocity.

[44] Although N^2 is relatively easy to estimate at any time, it is not possible to estimate Q and track its changes during restratification because the velocity structure was not measured in sufficient detail. M^2 can be estimated in the mixed layer prior to restratification, but not subsequently

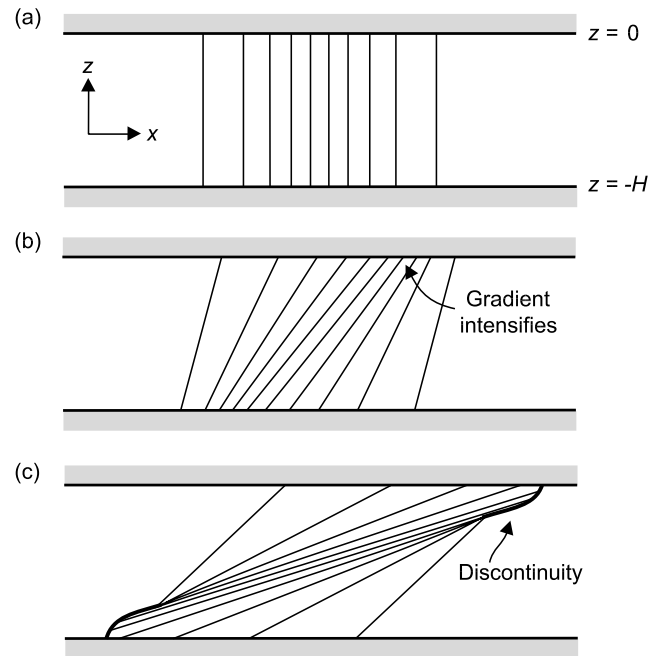


Figure 14. Sketch of the gravitational slumping of an uneven horizontal density gradient (shown by equally spaced isopycnals) in a layer bounded above and below by rigid surfaces. (a) Initially, the mid-depth points are in geostrophic balance, and the along-front velocity is vertically uniform, so an unbalanced pressure gradient drives a restratification in which isopycnals pivot about the mid-depth. (b) Isopycnals slump most rapidly where the horizontal density gradient is greatest. (c) Intensification of gradients by differential slumping leads to discontinuity in the density field at the surface and base of the restratifying layer (bold curves) (adapted from *Ou* [1984]).

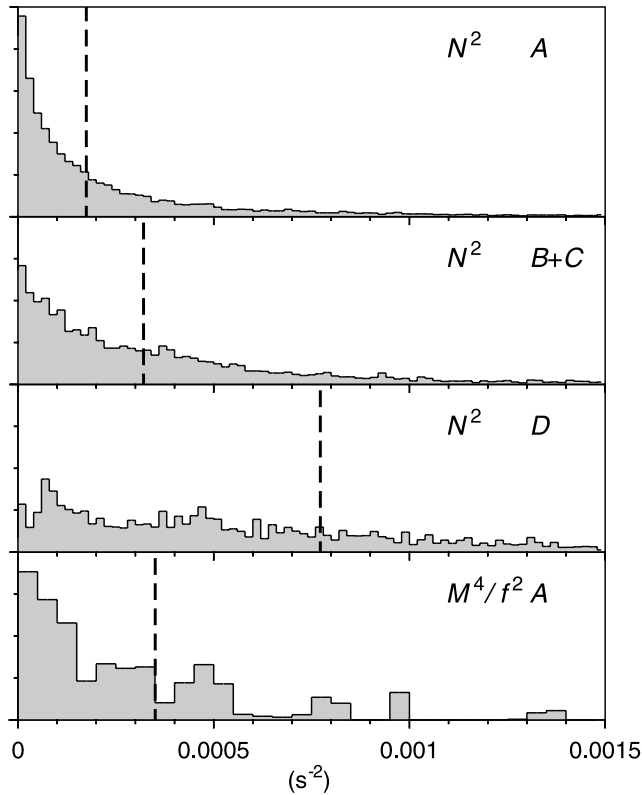


Figure 15. Histograms of the distribution of N^2 within the dye patch in time brackets containing transects A, B + C, and D. All are weighted by dye concentration. The lower panel shows M^4/f^2 , calculated in the time bracket containing transect A. Vertical dashed lines show the mean of each distribution. The distributions are normalized to have equal area, so vertical axes are dimensionless.

due to contamination by internal waves (which do not necessarily modify Q , but the velocity shears that balance their distortion of the density structure were not resolved).

[45] Despite the difficulties of calculating potential vorticity, it is instructive to compare the apparent tendency for the dye-laden water to retain its weakly stratified signature with predictions for a Q -conserving fluid. This Q -conserving fluid is assumed to behave locally as described by *Tandon and Garrett* [1994], so M remains constant and x -derivatives are neglected. While this is clearly a poor assumption close to the most intense front, it is a better assumption in the dye-laden water where cross-shelf gradients are weaker.

[46] The notation Δ_g is used to denote the change of a quantity during a (frictionless) geostrophic adjustment from an initial state with $\partial v/\partial z = 0$, to a final state that is in thermal wind balance. Each fluid parcel satisfies

$$0 = \Delta_g Q = f \Delta_g N^2 + \Delta_g (\partial v / \partial z M^2), \quad (14)$$

so invoking the eventual thermal wind balance, $\partial v/\partial z = -M^2/f$, and assuming constant M ,

$$\Delta_g N^2 = \frac{M^4}{f^2}. \quad (15)$$

Averaging over the dye patch, weighted by dye concentration, equation (15) can be expressed as

$$\Delta_g \overline{N^2} = \frac{\overline{M^4}}{f^2} \equiv R \quad (16)$$

(defining R in terms of the dye-weighted mean $\overline{M^4}$). Distributions of N^2 (Figure 15) in time brackets containing transects A, B + C and D, show an increasing mean stratification of the dye patch $\overline{N^2}$ as expected.

[47] An estimate of the increase in $\overline{N^2}$ due to geostrophic adjustment, $R = 3.51 \times 10^{-4} \text{ s}^{-2}$, is obtained from equation (16) by calculating the dye-weighted mean $\overline{M^4}/f^2$ in the mixed layer during the survey of Figure 4 (Figure 15, bottom panel). Relative to this, the observed increase in $\overline{N^2}$ between A and B was $\Delta_{AB} \overline{N^2} = 0.42 R$ and between A and D was $\Delta_{AD} \overline{N^2} = 1.71 R$ (again, from the distributions of Figure 15).

[48] As mentioned in section 3.5, a geostrophic adjustment oscillates inertially about its final thermal wind state. In the *Tandon and Garrett* [1994] case, these oscillations are undamped, and the instantaneous excess of $\overline{N^2}$ over its initial value oscillates between 0 and $2R$. In more realistic cases, the inertial oscillations are damped and a Q -conserving system converges on the thermal wind state in which the net increase of $\overline{N^2}$ is R . The qualitative observation that the dye-laden water retained its weakly stratified signature was made in section 2.6. More quantitatively, the observed increase in stratification between transects A and D, of $1.71R$, exceeds that of the thermal wind state but lies within the bounds of the oscillating *Tandon and Garrett* solution. It is presumed that, in this less idealized case, the inertial oscillations are rapidly damped and the increase in stratification over the thermal wind state largely results from a moderate change in Q due to wind stress and frictional effects. This change in Q is not, however, sufficient to erase the weakly stratified signature that distinguishes the dye-laden water from its surroundings.

3.7. Gravity Current Propagation

[49] As the front slumped, it steepened to become a discontinuous step in density. The light surface water from offshore of the front was separated from the denser water over which it flowed by a sharp interface. Such cases are described by gravity current dynamics. The speed of a buoyant gravity current is controlled by processes at its head (the front), so the pressure gradient does not accelerate the flow indefinitely, even in a nonrotating system [*von Kármán*, 1940]. Frictional effects are also significant.

[50] Calculations in section 3.2 suggested that the surface front propagated onshore at $0.43\text{--}0.60 \text{ m s}^{-1}$. In the absence of rotation, the head of a buoyant gravity current propagates into a (deep) ambient fluid with a Froude number close to unity [*Shin et al.*, 2004] with respect to perturbations on the base of the buoyant layer. So, for a two-layer fluid, the speed of the head is $c_{gc} \approx (g'H)^{1/2}$ where $g' = g\Delta\rho/\rho$ is a reduced gravity and H is the thickness of the buoyant layer behind its head. An estimate of $(g'H)^{1/2}$ is made for transect C, on which the buoyant plume most closely resembled a classic gravity current with a near-uniform H . For $H = 6 \text{ m}$ and $g' = 9 \times 10^{-3} \text{ m s}^{-1}$, the estimated propagation speed is $c_{gc} = 0.23 \text{ m s}^{-1}$ relative to

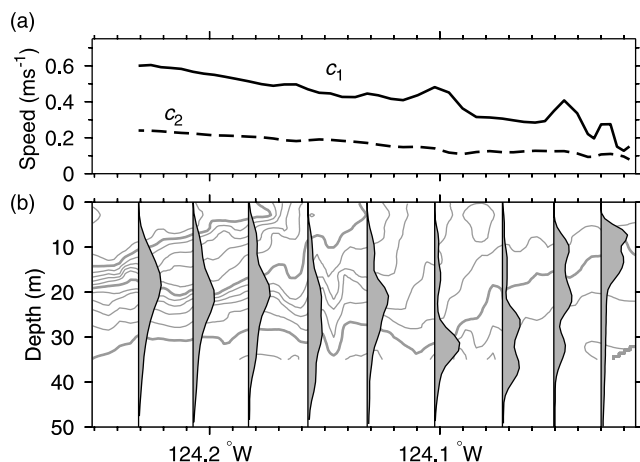


Figure 16. (a) Phase speed (c_1 , c_2) of the first two internal wave modes in the nondispersive limit, based on the stratification of transect B. (b) Mode 1 structure (as vertical velocity). Background contours are of density.

the ambient fluid. The ambient fluid was itself slumping onshore (Figure 8), at 0.22 m s^{-1} in the 8 m ADCP bin centered at 16 m beneath the surface front. The sum of these values, 0.45 m s^{-1} , predicts the onshore motion of the surface front, and lies toward the lower end of the range estimated from direct observations. The ambient velocity here is likely an underestimate, as shear in the slumping water column meant that the onshore velocity was greater closer to the surface. The drifter (drogued at 15 m) accelerated to 0.24 m s^{-1} onshore as the front approached (Figures 3, 7, and 12), confirming the ADCP velocity estimate.

[51] Of course, this was not a two-layer system. In particular, the ambient fluid itself contained a pycnocline at 20 m, the former base of the mixed layer, along which internal waves apparently propagated ahead of the front. It is hypothesized that these waves were generated by the adjustment of the ambient fluid to accommodate the front (compare, for example, with observations of wave generation at a river plume front, described by *Nash and Moun* [2006]). The presence of a stratified ambient fluid tends to reduce the speed of a gravity current, since energy can be lost to internal waves [*Ungarish and Huppert*, 2002]. Internal wave phase speeds for the observed stratification (Figure 16) have been calculated in the nondispersive limit (when frequency σ lies in the range $f^2 \ll \sigma^2 \ll N^2$) by direct solution of the vertical structure eigenvalue problem. Phase speed and group velocity are identical in this limit, and both decrease onshore as stratification weakens and the bottom shoals (Figure 16). Ahead of the front (at 124.15°W), the mode 1 phase speed is 0.45 m s^{-1} , which lies at the lower end of the estimated range of frontal propagation speed. This means that there was a tendency for onshore-propagating internal waves to be nearly stalled relative to the front, and for energy to build up in this region. Modal shapes (Figure 16) reveal that mode 1 was essentially an oscillation of the pycnocline at 20 m with maximum w in the range 15–35 m, consistent with the waves observed.

[52] The effects of rotation on the gravity current should not be neglected. Onshore motion induces an along-front

flow, as described by equation (10), with a 10 km onshore displacement leading to a 1 m s^{-1} southward velocity. This in turn leads to an offshore Coriolis acceleration which works to arrest the gravity current [e.g., *Hallworth et al.*, 2001]. Frictional effects on the base of the buoyant layer and the northward wind stress at the surface would both tend to weaken the southward flow permitting further onshore motion. Unfortunately, observations were not made of the velocity within the buoyant layer.

4. Discussion

4.1. Physical Evolution of the System

[53] The initial response to the weakening and reversal of upwelling-favorable winds was an onshore flow at the surface leading to a slumping of the density structure and a net onshore transport of the water that had previously formed the mixed layer. Two mechanisms have been identified as being potentially important: a wind-driven response to downwelling-favorable along-shelf winds, and a gravity-driven slumping due to imbalance in the cross-shelf pressure gradient. Baroclinic instability is known to be significant in mixed layer restratification [e.g., *Boccaletti et al.*, 2007], although it is assumed that it was not significant on the less than inertial timescale of the restratification described here.

[54] A key feature of the observed ocean response was its rapidity. Substantial onshore transport developed on time-scales that were much shorter than the inertial period (16.8 h). An onshore Ekman transport in response to along-shelf wind develops on the inertial timescale. In contrast, an unbalanced onshore pressure gradient drives an immediate onshore acceleration. In fact, geostrophic adjustment works to arrest such a flow on the inertial timescale. The differing time dependence of the two mechanisms favors the gravity-driven mechanism soon after wind reversal and the wind-driven mechanism subsequently.

[55] A model of gravitational slumping of a uniform density gradient [*Tandon and Garrett*, 1994] was used (section 3.5) to predict the rate of slumping of the density structure. Although slumping began as soon as the onshore pressure gradient was able to overcome vertical stirring, the timing of this event is difficult to estimate. It is presumed that it occurred close to the time when wind stress was a minimum, at wind reversal. The extent to which the water from the cross-shelf gradient maximum slumped during the first quarter of an inertial period after wind reversal is relatively well predicted by the model (at 4.2 km versus the observed 5.5 km displacement between the surface and base of the former mixed layer). The slight excess in the observed slumping may reflect the additional wind-driven contribution. In contrast, the net cross-shelf transport is not predicted by gravitational slumping. If a surface mixed layer is formed by vertically homogenizing the density and momentum of an upwelled density structure that is in geostrophic balance with a sheared jet [e.g., *Tandon and Garrett*, 1995], there is always a level within the interior of this layer that remains in balance. The unbalanced component of the pressure gradient changes sign at this level, and isopycnals pivot about it during restratification. Although there is a surface flow toward denser water, there may be no net cross-frontal transport of the former mixed layer. Such a

mechanism does not resolve the transport deficit in the wind-driven estimates.

[56] In the observations, isopycnals appeared to pivot about the base of the mixed layer and there was a net onshore transport of former mixed layer water. The reason for this may be that wind-induced mixing actually penetrates beneath the mixed layer. This would mean a deeper imbalance if the mixing were to suddenly stop, and a deeper pivot point for the restratification. *Lentz* [1992] observed that 25–50% of Ekman transport in an upwelling regime occurs beneath the mixed layer, implying that stress is transmitted to these depths. In the present case, the along-shelf velocity structure of the mixed layer was not known prior to wind reversal, so further investigation of the cross-shelf momentum balance is not possible. However, the evidence that points to an early dominance of gravity-driven restratification is strong: the timescale of the response, the deficit of predicted wind-driven transport and the favorable comparison of the extent of slumping with a simple model. In addition, a gravity-driven restratification provides a mechanism [*Ou*, 1984; *Tandon and Garrett*, 1994] by which frontal gradients can rapidly steepen, as was observed.

[57] Nonuniformity of the cross-shelf density gradient meant that the slumping front was preconditioned to steepen until it became an essentially discontinuous step in surface density. Gravity current theory can be applied to the subsequent onshore flow of Columbia-influenced water. The advance of the surface expression of the front was well predicted by a sum of the expected gravity current propagation speed and the onshore motion of the ambient fluid inshore of and beneath it. The extent to which a horizontal gradient can slump is ultimately limited by its coming into a state of geostrophic equilibrium, in thermal wind balance with along-front flow induced by rotation. There is a tendency to oscillate about this balanced state, unless further slumping is permitted by modification of potential vorticity. It is presumed that frictional stresses between the relatively thin (6-m) buoyant plume and the underlying ambient fluid, and the effect of ongoing downwelling-favorable wind stress, were significant for the plume, permitting its onshore advance to continue until it reached the coast (not observed). Downwelling-favorable wind stress may also have contributed to sharpening and maintaining the front because an onshore increase in the Ekman layer thickness would lead to a velocity convergence.

[58] If the water inshore of the front was itself slumping due to gravity, the limit imposed on this slumping by potential vorticity would mean that the eventual subduction of this water beneath the head of the advancing gravity current was inevitable provided that frictional and wind-induced stresses were not able to modify potential vorticity sufficiently to permit further slumping. Evidence, from tracking the dye patch, suggests that this water largely retained its low potential vorticity (weakly stratified) signature.

[59] As described in section 2.4, the restratification occurred in the context of an accelerating barotropic flow to the north. Such a barotropic response is typical in this region during wind relaxations or reversals, and is a result of along-shelf gradients [*Oke et al.*, 2002], although it is essentially decoupled from the baroclinic dynamics considered here.

4.2. How Typical Is Such a Wind Event?

[60] The frequency of wind events of the type described is investigated using 4 years (2001–2004) of data from NDBC buoy 46029 during the peak upwelling months of May–September. In this data set as a whole, the split between upwelling-favorable and downwelling-favorable winds is 68.4% to 31.6%. Strongly upwelling favorable winds ($\tau^y < -0.1 \text{ N m}^{-2}$) occurred 8.5% of the time and strongly downwelling-favorable winds ($\tau^y > 0.1 \text{ N m}^{-2}$) occurred 2.8% of the time. On only two occasions during these 20 upwelling months did strongly upwelling-favorable winds reverse to become strongly downwelling-favorable in less than an inertial period (16.8 h). It is one of these two events that is described here. Hourly averaged τ^y from the R/V *New Horizon* actually changed from -2.3 N m^{-2} to 1.9 N m^{-2} in just 13 h, making this a rather extreme event. Wind relaxations, however, are much more common, averaging more than two per month during this period. There were 44 events in which strongly upwelling favorable winds ($\tau^y < -0.1 \text{ N m}^{-2}$) became weak or reversed ($\tau^y > -0.01 \text{ N m}^{-2}$) in less than an inertial period.

[61] Physically, the key difference between wind relaxation and wind reversal is in the potential for direct onshore Ekman transport to develop. A gravity-driven restratification could occur during a wind relaxation with no reversal. The necessary precondition is that the preceding winds are sufficiently strong to create a mixed layer (here, 10 to 20 m thick) in which the cross-frontal pressure gradient is unbalanced because vertical momentum transfer prevents a thermal wind balance from being established. A purely gravity-driven slumping is ultimately arrested by rotation, unless downwelling-favorable winds or friction allow onshore transport to persist (effectively by modifying potential vorticity).

[62] The fact that the system experiences many relaxation events in the course of an upwelling season is significant. Asymmetry between the physics of upwelling and relaxation/downwelling [e.g., *Send et al.*, 1987] means that transports occurring during a relaxation/downwelling event are not exactly erased by the subsequent resumption of upwelling. A net cross-shelf transport results from repeated cycles of this sort [*Kuebel Cervantes et al.*, 2004].

4.3. Further Implications

[63] The Oregon upwelling system has high biological productivity which is strongly controlled by physical processes [*Menge et al.*, 2003]. Mechanisms that redistribute nutrients and organisms in the secondary (cross-shelf) sense are of particular interest (for example, in their ability to deliver larvae to the coast). Two types of phenomena that are seen in chlorophyll fields on the Oregon shelf, but whose origins are not well understood physically, are described below.

[64] First, anomalously warm, chlorophyll-rich layers are frequently observed in the base of the pycnocline offshore of the upwelling front. These features connect to the surface on the inshore side of the front [*Patullo and McAlister*, 1962; *Pak et al.*, 1970; *Stevenson et al.*, 1974; *Mooers et al.*, 1976], resembling the dye patch on line B (Figure 5). These features suggest a subductive pathway for surface waters [*Mooers et al.*, 1976]. Whether they are formed rapidly during relaxation events (as suggested by *Stevenson et al.*

[1974]), as a result of gradual secondary circulation during periods of sustained upwelling, by sheared along-shelf advection, or by internal tidal effects, is unclear. The present observations illustrate the potential for rapid subduction of surface water during wind relaxations. In these observations, however, the subducted surface water was overlain by mixed layer water from offshore. This is not the case for the anomalously warm layers which are usually overlain by cool water that is not of mixed layer origin.

[65] Second, and at a smaller scale (1 m or less vertically), thin plankton layers are frequently observed in vertical profiles [e.g., *Donaghay et al.*, 1992; *Cowles*, 2003]. While there are many processes that could create such features, the present observations illustrate a physical mechanism by which a widely distributed and relatively thick (>10 m) tracer layer (the dye patch in the mixed layer prior to wind reversal) was rapidly deformed by vertically sheared flow during restratification. The result was, in places, a thin, subsurface dye layer of just 1 to 2 m thick (Figure 6) forming a distinct layer within the pycnocline.

5. Conclusions

[66] The restratification of a mixed layer upwelling front was observed after sustained and strongly upwelling-favorable (southward) winds weakened and became downwelling-favorable (northward). This restratification took the form of an onshore transport of near-surface water, much of which occurred well within an inertial period (16.8 h) of the wind reversal.

[67] Two mechanisms are suspected to have made important contributions to this restratification: a wind-driven Ekman transport in response to downwelling-favorable along-shelf winds, and a gravity-driven slumping due to imbalance in the cross-shelf pressure gradient. Significantly, the timing of these contributions would differ. An Ekman transport develops over inertial timescales following wind reversal, whereas a gravity-driven transport accelerates as soon as the pressure gradient is able to overcome wind stirring (presumably close to the time of wind reversal). For this reason, the gravity-driven mechanism appears to have been responsible for the significant restratification that took place within a few hours of wind reversal. Calculations confirm that, in a simple model, the onset of wind-driven transport does not occur sufficiently soon after wind reversal to produce the observed onshore displacement of the density structure.

[68] Soon after wind reversal, cross-shelf gradients steepened as a result of nonuniformity of the initial cross-shelf density gradient [*Ou*, 1984]. Within a few hours, the surface front was effectively a step discontinuity which propagated onshore as the head of a buoyant gravity current with a thickness of 6 m. The $0.43\text{--}0.60\text{ m s}^{-1}$ progress of the front was a superposition of the gravity current propagation speed, at a predicted 0.23 m s^{-1} relative to the ambient fluid inshore of it, and onshore movement of the ambient fluid itself.

[69] Mixed layer water from inshore of the front detached from the surface and was subducted into the interior as the front passed over the top of it. This process was directly observed, in a Lagrangian frame, by tracking a patch of dye-laden water. Qualitatively, this water appeared to retain the weakly stratified signature that it had acquired in the mixed

layer. Although the velocity structure was not known well enough to explicitly calculate potential vorticity, the mean increase in stratification of the dye patch was within the bounds of a potential vorticity conserving geostrophic adjustment.

[70] Propagating onshore ahead of the surface front were internal waves of up to 8 m peak to trough amplitude on the base of the former mixed layer (at a depth of 20 m). Since the calculated first mode internal wave phase speed was close to the speed of the front, this disturbance was effectively locked to the front.

[71] Wind reversals of the rapidity and magnitude associated with this event are rather uncommon; it was the most extreme event of its type in the period 2001–2004. Wind relaxations, on the other hand, in which the wind weakens but does not reverse, are much more frequent. When strong winds lead to the formation of a substantial mixed layer, a wind reversal is not required for the slumping and gravity current propagation described here. A wind relaxation is sufficient.

[72] Perhaps the most important conclusion from the perspective of cross-shelf transport is that the onshore motion of near-surface water during this relaxation event was predominantly of water from offshore of the upwelling front. The denser, previously upwelled water from inshore of the front moved relatively little cross-shelf as the lighter, offshore water passed over the top of it. Beneath the mixed layer over the mid and outer shelf, the upwelled isopycnals and equatorward jet typical of coastal upwelling tend to remain essentially in place through relatively short wind relaxations and reversals [*Barth et al.*, 2005; *Austin and Barth*, 2002].

[73] **Acknowledgments.** This work was supported by NSF grant OCE-0136900. Startup funding for pilot experiments was provided by the G. Unger Vetlesen Foundation. The authors wish to thank Dennis Root for the design and construction of the dye-related apparatus, Anatoli Erofeev for coding real-time visualization software, Stephen Pierce for overseeing ADCP data collection and processing, Scripps resident technician Cambria Colt, Captain Murray Stein, and the crew of the R/V *New Horizon*.

References

- Allen, J. S., and P. K. Kundu (1978), On the momentum, vorticity and mass balance on the Oregon shelf, *J. Phys. Oceanogr.*, **8**, 13–27.
- Austin, J. A., and J. A. Barth (2002), Variation in the position of the upwelling front on the Oregon shelf, *J. Geophys. Res.*, **107**(C11), 3180, doi:10.1029/2001JC000858.
- Barth, J. A. (1994), Short-wavelength instabilities on coastal jets and fronts, *J. Geophys. Res.*, **99**, 16,095–16,115.
- Barth, J. A., S. D. Pierce, and R. M. Castelao (2005), Time-dependent, wind-driven flow over a shallow midshelf submarine bank, *J. Geophys. Res.*, **110**, C10S05, doi:10.1029/2004JC002761.
- Boccaletti, G., R. Ferrari, and B. Fox-Kemper (2007), Mixed layer instabilities and restratification, *J. Phys. Oceanogr.*, **37**, 2228–2250.
- Cooper, A. L., R. P. Mied, and G. L. Lindemann (2001), Evolution of freely propagating, two-dimensional gravity current fronts, *J. Geophys. Res.*, **106**, 16,887–16,901.
- Cowles, T. J. (2003), Planktonic layers: Physical and biological interactions on the small scale, in *Handbook of Scaling Methods in Aquatic Ecology: Measurements, Analysis, Simulation*, edited by L. Seuront and P. G. Strutton, pp. 31–49, CRC Press, Boca Raton, Fla.
- Csanady, G. T. (1971), On the equilibrium shape of the thermocline in a shore zone, *J. Phys. Oceanogr.*, **1**, 263–270.
- Dale, A. C., M. D. Levine, J. A. Barth, and J. A. Austin (2006), A dye tracer reveals cross-shelf dispersion and interleaving on the Oregon shelf, *Geophys. Res. Lett.*, **33**, L03604, doi:10.1029/2005GL024959.
- D'Asaro, E. A. (1985), The energy flux from the wind to near-inertial motions in the surface mixed layer, *J. Phys. Oceanogr.*, **15**, 1043–1059.

- Donaghay, P. L., H. M. Rines, and J. M. Seiburth (1992), Simultaneous sampling of fine scale biological, chemical and physical structure in stratified waters, *Ergeb. Limnol.*, *36*, 97–108.
- Durski, S. M., and J. S. Allen (2005), Finite amplitude evolution of instabilities associated with the upwelling front, *J. Phys. Oceanogr.*, *35*, 1606–1628.
- Hallworth, M. A., H. E. Huppert, and M. Ungarish (2001), Axisymmetric gravity currents in a rotating system: Experimental and numerical investigations, *J. Fluid Mech.*, *447*, 1–29.
- Houghton, R. W. (1997), Lagrangian flow at the foot of a shelfbreak front using a dye tracer injected into the bottom boundary layer, *Geophys. Res. Lett.*, *24*, 2035–2038.
- Huyer, A., E. C. Sobey, and R. L. Smith (1979), The spring transition in currents over the Oregon continental shelf, *J. Geophys. Res.*, *84*, 6995–7011.
- Kelly, K. A. (1985), The influence of winds and topography on the sea surface temperature patterns over the Northern California shelf, *J. Geophys. Res.*, *90*, 11,783–11,798.
- Kuebel Cervantes, B. T., J. S. Allen, and R. M. Samelson (2004), Lagrangian characteristics of continental shelf flows forced by periodic wind stress, *Nonlinear Process. Geol.*, *11*, 3–16.
- Lentz, S. J. (1992), The surface boundary layer in coastal upwelling regions, *J. Phys. Oceanogr.*, *22*, 1517–1539.
- Menge, B. A., et al. (2003), Coastal oceanography sets the pace of rocky intertidal community dynamics, *Proc. Natl. Acad. Sci. U. S. A.*, *100*, 12,229–12,234.
- Mooers, C. N. K., C. A. Collins, and R. L. Smith (1976), The dynamic structure of the frontal zone in the coastal upwelling region off Oregon, *J. Phys. Oceanogr.*, *6*, 3–21.
- Nash, J. D., and J. N. Moum (2006), River plumes as a source of large amplitude internal waves in the coastal ocean, *Nature*, *437*, 400–403, doi:10.1038/nature03936.
- Oke, P. R., J. S. Allen, R. N. Miller, and G. D. Egbert (2002), A modeling study of the three-dimensional continental shelf circulation off Oregon. part II: Dynamical analysis, *J. Phys. Oceanogr.*, *32*, 1383–1403.
- Ou, H. W. (1984), Geostrophic adjustment: A mechanism for frontogenesis, *J. Phys. Oceanogr.*, *14*, 994–1000.
- Pak, H., G. F. Beardsley, and R. L. Smith (1970), An optical and hydrographic study of a temperature inversion off Oregon during upwelling, *J. Geophys. Res.*, *75*, 629–636.
- Patullo, J. G., and W. B. McAlister (1962), Evidence for oceanic frontogenesis off Oregon, *Science*, *135*, 106–107.
- Pedlosky, J. (1979), *Geophysical Fluid Dynamics*, 624 pp., Springer, New York.
- Pollard, R. T., and R. C. Millard (1970), Comparisons between observed and simulated wind-generated inertial currents, *Deep Sea Res.*, *17*, 813–821.
- Roughgarden, J., J. T. Pennington, D. Stoner, S. Alexander, and K. Miller (1991), Collisions of upwelling fronts with the intertidal zone: The cause of recruitment pulses in barnacle populations of central California, *Acta Oecol.*, *12*, 35–51.
- Send, U., R. C. Beardsley, and C. D. Winant (1987), Relaxation from upwelling in the Coastal Ocean Dynamics Experiment, *J. Geophys. Res.*, *92*, 1683–1698.
- Shin, J. O., S. B. Dalziel, and P. F. Linden (2004), Gravity currents produced by lock exchange, *J. Fluid Mech.*, *521*, 1–34.
- Smart, P. L., and I. M. S. Laidlaw (1977), An evaluation of some fluorescent dyes for water tracing, *Water Resour. Res.*, *13*, 15–33.
- Smith, R. L. (1974), A description of current, wind, and sea level variations during coastal upwelling off the Oregon coast, July–August 1972, *J. Geophys. Res.*, *79*, 435–443.
- Stevenson, M. R., R. W. Garvine, and B. Wyatt (1974), Lagrangian measurements in a coastal upwelling zone off Oregon, *J. Phys. Oceanogr.*, *4*, 321–336.
- Sundermeyer, M. A., and J. R. Ledwell (2001), Lateral dispersion over the continental shelf: Analysis of dye release experiments, *J. Geophys. Res.*, *106*, 9603–9622.
- Tandon, A., and C. Garrett (1994), Mixed layer restratification due to a horizontal density gradient, *J. Phys. Oceanogr.*, *24*, 1419–1424.
- Tandon, A., and C. Garrett (1995), Geostrophic adjustment and restratification of a mixed layer with horizontal gradients above a stratified layer, *J. Phys. Oceanogr.*, *25*, 2229–2241.
- Ungarish, M., and H. E. Huppert (2002), On gravity currents propagating at the base of a stratified ambient, *J. Fluid Mech.*, *458*, 283–301.
- von Kármán, T. (1940), The engineer grapples with nonlinear problems, *Bull. Am. Math. Soc.*, *46*, 615–683.
- Young, W. R. (1994), The subinertial mixed layer approximation, *J. Phys. Oceanogr.*, *24*, 1812–1826.

J. A. Austin, Large Lakes Observatory, University of Minnesota, Duluth, MN 55812, USA.

J. A. Barth and M. D. Levine, College of Oceanic and Atmospheric Sciences, Oregon State University, Corvallis, OR 97331-5503, USA.

A. C. Dale, Scottish Association for Marine Science, Dunstaffnage Marine Laboratory, Oban, Argyll PA37 1QA, UK. (andrew.dale@sams.ac.uk)